Journal of Autoimmunity 96 (2019) 168–177

Contents lists available at ScienceDirect

Journal of Autoimmunity

journal homepage: www.elsevier.com/locate/jautimm

Structural mapping of hot spots within human CASPR2 discoidin domain for autoantibody recognition

Wenjun Liang[a,b,1], Junying Zhang[a,b,1], Margaux Saint-Martin[c,d,e,1], Fei Xu[a,b], Nelly Noraz[c,d,e], Jianmei Liu[a,b], Jérôme Honnorat[c,d,e,**], Heli Liu[a,b,*]

[a] State Key Laboratory of Natural and Biomimetic Drugs & School of Pharmaceutical Sciences, Peking University Health Science Center, 38 Xueyuan Road, Haidian District, Beijing 100191, China
[b] Department of Molecular and Cellular Pharmacology, School of Pharmaceutical Sciences, Peking University Health Science Center, 38 Xueyuan Road, Haidian District, Beijing 100191, China
[c] French Reference Center on Paraneoplastic Neurological Syndrome, Hospices Civils de Lyon, Hôpital Neurologique, Bron, France
[d] INSERM U1217–CNRS UMR5310, NeuroMyoGene Institute, Lyon, France
[e] Université Claude Bernard Lyon 1, Université de Lyon, France

ARTICLE INFO

Keywords:
CASPR2
Discoidin domain
Crystal structure
Autoantibody
Limbic encephalitis

ABSTRACT

Accumulating evidence has showed that anti-CASPR2 autoantibodies occur in a long list of neurological immune disorders including limbic encephalitis (LE). Belonging to the well-known neurexin superfamily, CASPR2 has been suggested to be a central node in the molecular networks controlling neurodevelopment. Distinct from other subfamilies in the neurexin superfamily, the CASPR subfamily features a unique discoidin (Disc) domain. As revealed by our and others' recent studies, CASPR2 Disc domain bears a major epitope for autoantibodies. However, structural information on CASPR2 recognition by autoantibodies has been lacking. Here, we report the crystal structure of human CASPR2 Disc domain at a high resolution of 1.31 Å, which is the first atomic-resolution structure of the CASPR subfamily members. The Disc domain adopts a total β structure and folds into a distorted jellyroll-like barrel with a conserved disulfide-bond interlocking its N- and C-termini. Defined by four loops and located in one end of the barrel, the "loop-tip surface" is totally polar and easily available for protein docking. Based on structure-guided epitope prediction, we generated nine mutants and evaluated their binding to autoantibodies of cerebrospinal fluid from twelve patients with limbic encephalitis. The quadruple mutant G69N/A71S/S77N/D78R impaired CASPR2 binding to autoantibodies from eleven LE patients, which indicates that the loop L1 in the Disc domain bears hot spots for autoantibody interaction. Structural mapping of autoepitopes within human CASPR2 Disc domain sheds light on how autoantibodies could sequester CASPR2 ectodomain and antagonize its functionalities in the pathogenic processes.

1. Introduction

As a fascinating advancement in the field of neuroimmunology in the last decade, accumulating evidence has revealed that a wide range of neurological diseases are mediated by autoantibodies against neuronal cell surface proteins involved in synaptic signaling and plasticity [1–3]. Among the neuronal cell-surface antigens, CASPR2 is an attractive one, since anti-CASPR2 autoantibodies have been reported in a long list of neurological immune disorders including Morvan's syndrome and limbic encephalitis [4–17]. Our recent cohort study has showed that anti-CASPR2 antibodies in the cerebrospinal fluid (CSF) are closely associated with a subtype of autoimmune encephalitis with prominent limbic involvement and seizures [18].

Human CASPR2 encoded by the *CNTNAP2* gene, is a 1331-residue long and single-passing transmembrane protein that contains an N-terminal signal peptide followed by an extracellular region, one transmembrane domain and a short C-terminal intracellular region. The extracellular region is composed of a mosaic of domains, including the N-terminal discoidin (Disc), laminin G (Lam1), laminin G (Lam2), epidermal growth factor 1 (Egf1), fibrinogen C (FibC), laminin G

* Corresponding author. State Key Laboratory of Natural and Biomimetic Drugs & School of Pharmaceutical Sciences, Peking University Health Science Center, 38 Xueyuan Road, Haidian District, Beijing 100191, China.
** Corresponding author. French Reference Center on Paraneoplastic Neurological Syndrome, Hospices Civils de Lyon, Hôpital Neurologique, Bron, France.
E-mail addresses: jerome.honnorat@chu-lyon.fr (J. Honnorat), liuheli@hsc.pku.edu.cn (H. Liu).
[1] These authors contributed equally.

https://doi.org/10.1016/j.jaut.2018.09.012
Received 31 May 2018; Received in revised form 23 September 2018; Accepted 30 September 2018
Available online 15 October 2018
0896-8411/

(Lam3), Egf (Egf2), and laminin G (Lam4) domains [19]. As a cell-adhesion molecule, CASPR2 belongs to the neurexin superfamily; however, distinct from other members in the neurexin superfamily, the CASPR subfamily members, including CASPR1 through CASPR5 (also named CNTNAP1-CNTNAP5), contain a Disc domain [19]. Like neurexin which is well-known for functioning in synapse formation and association with neurological disorders such as autism [20], CASPR2 plays an important role for neuronal dendritic arborization, spine morphology and synaptic formation [21–23], while mutations in the *CNTNAP2* gene encoding CASPR2 were mainly identified in patients with focal epilepsy, intellectual disability, or autism [24–26]. Worthy to mention, a high concentration of mutations was found in the exons coding for the discoidin domain [27]. In addition, knockout of the *CNTNAP2* gene led to deficits in the core ASD behavioral domains in a mouse model [28]. Multiple-domain organization in CASPR2 implicates that it may engage in a number of protein-protein interactions to regulate functions [29]. Likely owing to multifaceted functions and involvement in extensive protein interactions, CASPR2 has been suggested to be a central node in the molecular networks controlling neurodevelopment [30].

Mapping anti-CASPR2 antibody epitope(s) at the structural level would facilitate revealing mechanisms for autoantibody pathogenicity and improve diagnosis and treatment for CASPR2-associated autoimmune diseases such as limbic encephalitis [31]. Using the cell-based binding and neuron-based functional assays, we have showed that anti-CASPR2 antibodies from a subtype of limbic encephalitis patients selectively reacted with the N-terminal modules, including Disc and Lam1 domains of CASPR2, and that anti-CASPR2 antibodies mainly target hippocampal inhibitory interneurons and may induce alteration of CASPR2-mediated inhibitory synaptic contacts [32]. Deletion of the Disc domain of CASPR2 showed significantly reduced immunoreactivity against antibody-positive patient sera, even though without a complete abrogation of binding [33]. This report further suggests that the Disc domain of CASPR2 contains a major epitope for autoantibodies.

Although molecular architecture of the full-length ectodomain of CASPR2 was constructed by electron microscopy [34,35], no high-resolution structure has been determined for any domain of CASPR2. Structural information on CASPR2 interacting with autoantibodies has also been lacking. Here, we report the crystal structure of human CASPR2 Disc domain at 1.31 Å resolution, which to our best knowledge is the first atomic-resolution structure for the CASPR subfamily. Using structure-guided mutagenesis and protein-based ELISA, we have revealed hot spots within the Disc domain for recognition by anti-CASPR2 autoantibodies from patients with limbic encephalitis. Hopefully, these findings may shed light on how autoantibodies could antagonize CASPR2's functionalities in the pathogenic processes.

2. Methods

2.1. Molecular cloning and baculovirus generation

cDNA fragments encoding the Disc domain (amino-acid residues 35–181) of human CASPR2 (NCBI Reference Sequence: NM_014141.5) were amplified by PCR using gene-specific primers containing *Bam*HI and *Not*I sites. The PCR fragments were subsequently digested and ligated into a modified BacMam vector [36,37]. A hexahistidine tag was introduced to the C-terminus of the construct to facilitate protein purification. After being verified by DNA sequencing, plasmids were co-transfected with BacVector-3000 baculovirus DNA (EMD, USA) using Cellfectin (Life technologies, USA) into *sf9* insect cells in the serum and antibiotics-free SF900-II media (Life technologies, USA). Primary progeny of recombinant virus was used to infect *sf9* cells for amplification. 6 d later, higher-titer baculovirus was harvested by centrifugation at 1000*g* for 10 min.

2.2. Protein expression and purification

For protein expression, an appropriate volume of recombinant baculovirus was used to transduce HEK293S cells cultured in the DMEM/F12 (Gibco, USA) media supplemented with 10% FBS (Life technologies, USA). 72 h post viral transduction, the conditioned medium was centrifuged at 3000 g at 277 K for 15 min. The supernatant was harvested, buffer-exchanged to HBS (HEPES-buffered saline, containing 10 mM HEPES pH 7.5 and 150 mM NaCl) and applied to Ni^{2+}–NTA affinity chromatography. The unbound proteins were subsequently removed from the affinity column using washing buffer (HBS supplemented with 20 mM imidazole). The affinity column eluate from 300 mM imidazole-containing HBS was further applied to a Superdex-200 10/300 GL size-exclusion column (GE Healthcare) pre-equilibrated with HBS. The fractions eluted at 17–18 ml were verified by SDS-PAGE with Coomassie blue staining, pooled and concentrated to 10 mg/ml for crystallization. The protein concentration was determined through measuring OD_{280} values and calculated with extinction coefficients of 46535 $M^{-1}{\cdot}cm^{-1}$.

2.3. Crystallization

The initial crystallization conditions were screened at 293 K by the sitting-drop vapor-diffusion method using the Hampton kit (HR2-130) and the Emerald Biosystems kit (Wizard I and II). 3 d later, microcrystals were found in the No. 8 condition of the Wizard Classic kit II. After optimization, diffraction-quality brick-like crystals, with a typical dimension of $0.2 \times 0.2 \times 0.3\ mm^3$, were obtained from a sitting drop in equilibration with the reservoir solution consisting of 20% (w/v) PEG8000, 100 mM Na_2HPO_4/KH_2PO_4 (pH 6.2) and 200 mM NaCl.

2.4. Data collection and structure determination

Crystals were fast-soaked in the crystallization solution supplemented with 22–24% (v/v) ethylene glycerol prior to being flash-cooled in liquid nitrogen. Diffraction data were collected on the beamline BL19U1 at Shanghai Synchrotron Radiation Facility (SSRF). The data sets were indexed and processed using HKL2000 [38]. Phases were calculated with molecular replacement (MR) method in PHASER [39]. The crystal structure of the membrane-binding C2 domain of human coagulation factor V (PDB code: 1CZV) [40] was used as a template for searching MR solution. The resulting solution, with a TFZ score of 15.3, was subjected to Autobuild in the software PHENIX [41]. The auto-built model was improved by iterative manual building in COOT [42] and refinement in PHENIX. During the final stage of refinement, water molecules were introduced using PHENIX and manually edited in COOT. The stereochemistry of the final model was evaluated using Molprobity [43]. The statistics for data collection and refinement are given in Table 1.

2.5. Epitope prediction and structure analysis

The crystal structure of human CASPR2 Disc domain was applied to DiscoTope 2.0 server [44] for epitope prediction, with the threshold for epitope identification set at −3.7. For structure analysis, DALI [45] was used to search for structural homology. Structure-based sequence alignment was executed using ClusterW [46] and mapped using ESPRIPT [47]. Conservation of residues was based on chemical character: aromatic (F, Y, and W), hydrophobic (L, I, V, and M), acidic (E and D), basic (K, R, and H), polar (S and T), tiny (G and A), and amide (N and Q). Conservation was mapped to protein surface using Consurf [48]. Solvent accessible surface area for each atom was calculated using the program AREAIMOL in the CCP4 suite [49].

Table 1
Data collection and refinement statistics for human CASPR2 Disc domain.

Data collection	
X-ray source	SSRF BL19U1
Detector	Pilatus3 6M
Wavelength (Å)	0.978
Crystal-to-detector distance (mm)	200
Oscillation range (°)	180
Oscillation width per image (°)	1
Space group	$P2_12_12_1$
Unit cell dimensions: a, b, c (Å); α, β, γ (°)	36.250, 59.680, 62.599; 90, 90, 90
Resolution range (Å)[a]	50–1.31 (1.33–1.31)
Unique reflections	33381 (1598)
Completeness (%)	99.6 (97.3)
$I/\sigma(I)$	35.4 (2.75)
Redundancy	8.5 (6.1)
R_{merge} (%)[b]	7.8 (53.8)
R_{meas} (%)[b]	8.3 (58.6)
R_{pim} (%)[b]	2.8 (22.7)
Refinement	
Resolution range (Å)	31.37–1.31 (1.36–1.31)
R_{work}[c]	13.33 (15.99)
R_{free}[c]	16.51 (21.11)
Average *B*-factor for protein and solvent (Å^2)	19.99, 34.17
r.m.s.d. bond length (Å)	0.01
r.m.s.d. bond angle (°)	1.18
Ramachandran (%; favored, allowed, generally allowed, disallowed)	98.7, 1.3, 0, 0

[a] Values in parenthesis are for the highest resolution shell.
[b] $R_{merge} = \Sigma_{hkl}|I - \langle I\rangle|/\Sigma_{hkl}I$, where I is the intensity of unique reflection *hkl*, and $\langle I\rangle$ is the average over symmetry-related observations of unique reflection *hkl*. R_{pim}: precision-indicating merging R-factor. R_{meas}: multiplicity-corrected merging R-factor.
[c] $R_{work} = \Sigma|F_o - F_c|/\Sigma|F_o|$, where F_o and F_c are the observed and calculated structure factors, respectively. R_{free} was calculated using 5% of the reflections set aside from refinement.

2.6. Structure-based mutagenesis

cDNAs encoding human CASPR2 Disc domain plus the N-terminal segment (residues 28-181) and its mutants S55N, G69N/A71S, S77N, D78R, Y82A, W134S, D143S, R171E and G69N/A71S/S77N/D78R were amplified by a single-step or two-step overlapping PCR. Subcloning, baculovirus recombination and protein preparation for these mutants were performed using the same protocol as used for the construct produced for crystallization.

2.7. Patients

Approval for this study was granted by the institutional review board of the Hospices Civils de Lyon (Comité de Protection des Personnes SUD-EST IV). Written informed consent was obtained from all patients. Titer, IgG subclass and target domains of the auto-antibodies directed against CASPR2 in the limbic encephalitis (LE) patient's CSF were previously characterized [18]. Twelve CSF samples with titers between 1:320 and 1:10240 were obtained from the NeuroBioTec biobank (Hospices Civils de Lyon, France). In these CSF samples, 6 had antibodies directed against the Disc and Lam1 domains only (Disc-Lam1) and 6 against multiple domains of CASPR2 (Mult). Basic immunological features of the LE patients are listed in Table 2.

2.8. Protein-based ELISA

Recombinant human CASPR2 Disc domain plus the N-terminal segment (residues 28-181), or its mutants, or BSA, was coated onto a 96-well plate (Costar 3590, Corning Incorporated) with 0.4 μg protein in 50 μl of Na_2CO_3/$NaHCO_3$ buffer (pH 9.5) per well for overnight incubation at 4 °C. The wells were each washed thrice with 200 μl of phosphate-buffered saline containing 0.05% Tween-20 (PBS-T), and blocked with 200 μl of PBS supplemented with 10% (v/v) fetal bovine serum (FBS) for 2 h at 37 °C. The blocking solution was then removed and 50 μl of CSF diluted in 2% (v/v) FBS-containing PBS was added. After further incubation at 37 °C for 2 h, the wells were washed three times with PBS-T, and incubated for 30 min at 37 °C with 50 μl of 2% (v/v) FBS-containing PBS in the presence of HRP-conjugated goat anti-human IgG antibodies (Jackson Immuno Research, Ref. 109-036-064) (diluted at 1:8000). After three washes in PBS-T, 50 μl of the TMB solution was added to each well (Abcam, AB171523). After 15 min, the reaction was stopped by the addition of 50 μl of 2M HCl. Optical densities (ODs) were recorded at 450 nm using a microplate reader (Tecan). Unless otherwise stated, experiments were performed in triplicate and the data were represented as a mean value ± standard deviation. The represented OD_{450} value was calculated using the OD value for coated Disc proteins subtracted by that for BSA (as a control). The OD decrease was considered significant when it was two times larger than the highest standard deviation (with a threshold set at 20%).

Table 2
Basic immunological features of LE patients with anti-CASPR2 antibodies.

Patient	Titer[a]	Dilution[b]	Epitope[c]
Pat1	1:1280	1:20	Disc-Lam1
Pat2	1:10240	1:100	Disc-Lam1
Pat3	1:640	1:10	Disc-Lam1
Pat4	1:1280	1:20	Disc-Lam1
Pat5	1:10240	1:100	Disc-Lam1
Pat6	1:5120	1:40	Disc-Lam1
Pat7	1:1280	1:20	Mult
Pat8	1:5120	1:40	Mult
Pat9	1:320	1:10	Mult
Pat10	1:2560	1:20	Mult
Pat11	1:10240	1:100	Mult
Pat12	1:5120	1:40	Mult

[a] CSF titers (last dilution of CSF giving a positive signal) were previously determined by cell based assay [18].
[b] Lowest dilution used in the ELISA.
[c] Disc-Lam1: for antibodies targeting the Disc and Lam1 domains only; Mult: antibodies targeting the Disc and Lam1 domains as well as other domains.

3. Results

3.1. Overall structure of the CASPR2 Disc domain

Using baculovirus-transduced mammalian cells, we obtained high-expression of human CASPR2 Disc domain (residues 35-181) and purified it into high homogeneity and purity (Fig. 1A). The recombinant protein had an elution volume of 17.7 ml, corresponding to an estimated molecular mass of ~14 kDa. The estimated molecular mass is close to the calculated value, 17.4 kDa, based on its primary sequence plus cloning scar and tag, which indicates that human CASPR2 Disc domain mainly exists as a monomer in solution. This is consistent with the previous report that the extracellular region of CASPR2 is likely monomeric [50]. The purified protein crystallized in the $P2_12_12_1$ space group, and diffracted to 1.31 Å (Table 1). Given the presence of one molecule of the Disc domain per asymmetric unit, the Matthews coefficient (V_M) was calculated to be 2.53 Å^3·Da^{-1}, corresponding to a reasonable solvent content of 51.3% [51]. Using the structure of the membrane-binding C2 domain of human coagulation factor V [40] as a template for molecular replacement, we solved the crystal structure of human CASPR2 Disc domain, and the final model has relatively low R_{work}/R_{free} factors and a reasonable stereochemistry (Table 1).

Human CASPR2 Disc domain adopts a total β structure and folds into a distorted jellyroll-like barrel, with a dimension of approximately 35 × 30 × 25 Å^3. This barrel mainly consists of eight antiparallel β-strands arranged in two sheets, with five strands β1, β2, β4, β5 and β7 forming one sheet packed against by the other one that is composed of

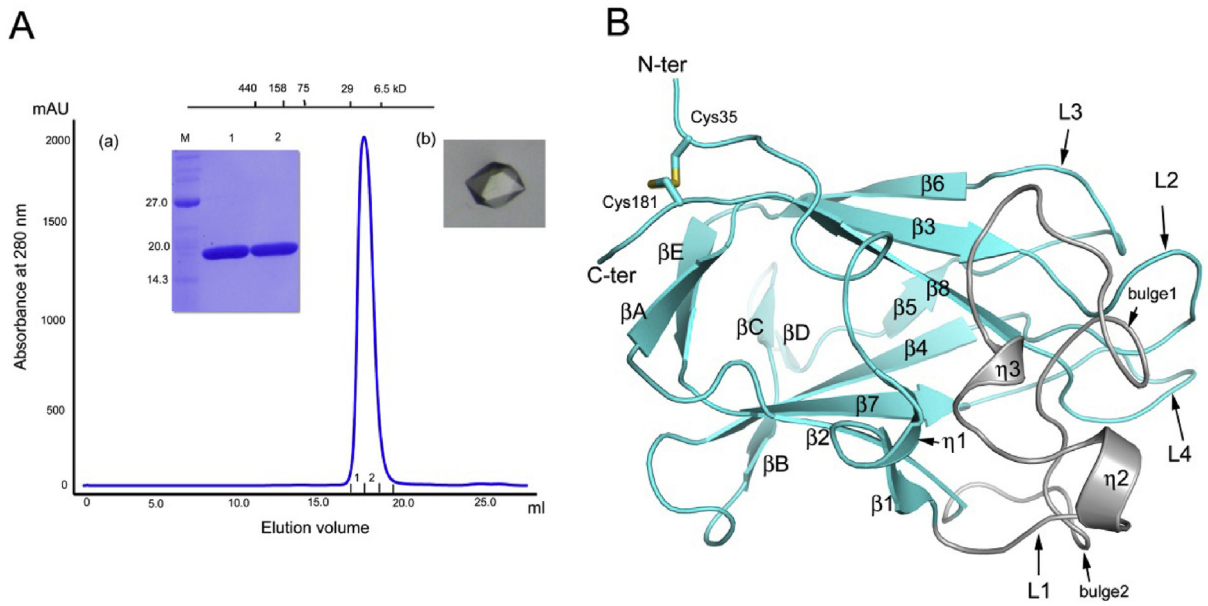

Fig. 1. Biochemical characterization and overall structure of human CASPR2 Disc domain. (A) Gel filtration chromatogram of recombinant human CASPR2 Disc domain. The inset (a) is an image for Coomassie blue-stained SDS-PAGE analysis of two fractions 1 and 2 eluted from a Superdex 200 gel filtration column. M, molecular weight marker in kDa. A crystal of the Disc domain is shown in the inset (b). (B) Ribbon representation of human CASPR2 Disc domain (in cyan) with secondary structure elements labeled and the loop L1 highlighted in grey. The N- and C-termini are respectively labeled as "N-ter" and "C-ter". The disulfide bond Cys35-Cys181 is indicated in sticks. (For interpretation of the references to color in this figure legend, the reader is referred to the Web version of this article.)

three strands β3, β6 and β8 (Fig. 1B). Different from other barrel-wall strands, the strand β5 follows a protruding hairpin that is composed of short strands βC and βD. The strand βC is proceeded by the strand βB which joins the barrel sheet and is antiparallel with the C-terminal half of the strand β4.

On one end of the barrel, the N-terminal residue Cys35 and the C-terminal residue Cys181 forms a disulfide bond that locks the barrel. Preceding the short strand β1, the N-terminal segment (residues 34-47) assumes a loop configuration with residues 45-47 folding into a short 3_{10} helix, η1. Adjacent to the C-terminal segment is an β-sheet of two antiparallel strands βA and βB. The strand βA connects the barrel-wall strands β2 and β3, while the strand βE is located in the middle of the link between the strands β6 and β7. The long axis of the βA/βE sheet is almost perpendicular to that of the barrel.

On the other end of the barrel are distributed four loops (named L1, L2, L3 and L4) each connecting the barrel-wall strands. The L1, linking the strands β1 and β2, is the longest and most twisted loop that contains residues 51–84 and folds into two short 3_{10} helices, η2 at residues 56-58 and η3 at residues 60-62. Noteworthy is that the L1 loop forms two bulges at residues 68-72 (for bulge1) and residues 76-78 (for bulge2), which flank the η2 helix (Fig. 1B). The loops L2 (connecting the strands β3 and β4) and L4 (connecting β6 and β7) are interlocking with each other. Meanwhile, the loop L2 is flanked by the loops L1 and L3 (linking β5 and β6), and the loop L1 adopts a concave configuration and half-wraps the loops L2 and L4 (Fig. S1). The tips of the loops L2, L3 and L4 are almost aligned to the same level with the two bulges and the η2 helix of L1, thus forming a relatively flat surface on one end of the barrel (Fig. S1).

3.2. Structural comparison of CASPR2 Disc domain and its homologues

The overall structure of human CASPR2 Disc domain is similar to that of the membrane-binding C2 domain of human coagulation factor V [40], with an RMSD value of 0.81 Å for 114 aligned C_α atoms. These aligned C_α atoms are mainly located in the barrel-wall strands, indicating that CASPR2 Disc and coagulation factor V C2 domains share the same folding (Fig. 2A). However, unlike the loops (such as L1 and L2) of human CASPR2 Disc domain that constitute a relatively flat

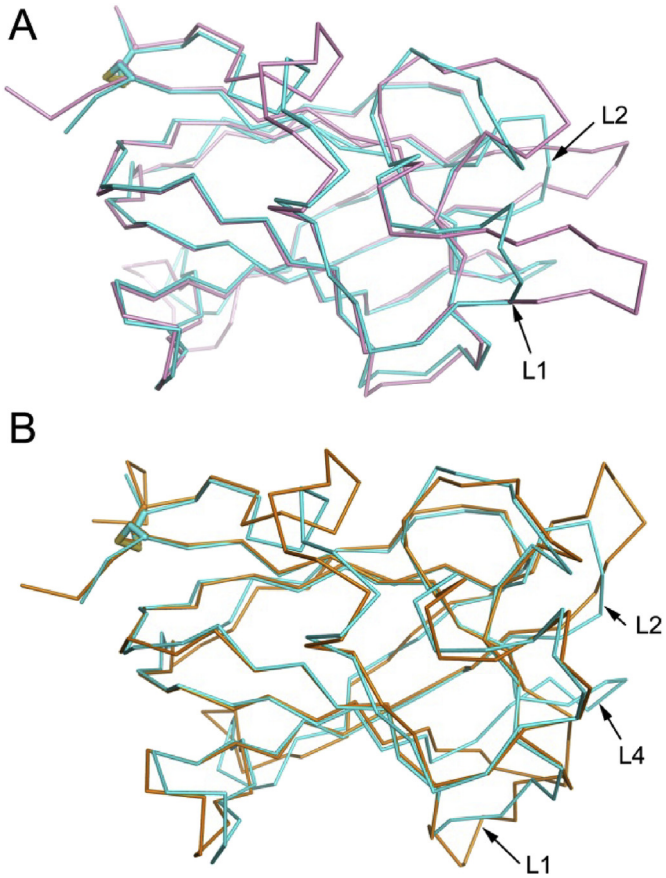

Fig. 2. Structural comparison of human CASPR2 Disc domain (in cyan) with homologues: (A), human coagulation factor V C2 domain (in pink); (B), DDR2 Disc domain (in orange). All structures are shown in cartoons, and the loops with large structural variations are labeled in CASPR2 numbering. (For interpretation of the references to color in this figure legend, the reader is referred to the Web version of this article.)

platform, the homologous counterparts in human coagulation factor V protrude like spikes [40] (Fig. 2A). As revealed by Dali search [45], the structure of the Disc domain of DDR2 (referring to Discoidin Domain Receptor 2; PDB code: 2wuh) [52] can also be superimposed with that of CASPR2 with an RMSD value of 0.75 Å for 127 paired C_α atoms, and their structural variation also mainly occurs to the loops such as L1, L2 and L4 (Fig. 2B). In comparison with human coagulation factor V C2 domain, the Disc domain of both CASPR2 and DDR2 has a compact and flat loop region that might facilitate docking to other proteins. Therefore, similar to the case of DDR2 where the loop region in the Disc domain engages in collagen recognition [52] (Fig. S2), CASPR2 Disc domain might utilize its loop region for protein recognition. Finally, in the human factor VIII C2 domain (PDB code: 1iqd), also able to overlay with CASPR2 Disc domain, the loop region was shown to bind to a patient-derived inhibitory antibody [53] (Fig. S2). This further implicates that the loop region defined by the loops L1-L4 in human CASPR2 Disc domain might constitute an epitope for recognition by other proteins, including autoantibodies.

3.3. Surface properties of human CASPR2 Disc domain

Defined by the loop L1-L4, the loop region is located in one end of the barrel-like human CASPR2 Disc domain, opposite to the other end containing the N- and C-termini. The solvent-accessible surface of this region, hereafter designated "loop-tip surface", is totally polar and hydrophilic, since it is mainly composed of the residues Ile54, Ser55, Ser57, Tyr58, Arg68, Gly69, Ala71, Ser77 and Asp78 from the loop L1, Arg103, Tyr104, Ser105, Ser107 and Asp108 from the loop L2, and Glu169 and Arg171 from the loop L4 (Fig. S1 and Fig. 3). Located in the center of the "loop-tip surface" is Arg103 that forms a salt bridge with Asp108. Around the edge of the "loop-tip surface" are distributed highly solvent-accessible hydrophilic residues such as Ser55, Arg68, Ser77, Asp78, Tyr104, Ser105, Ser107, Glu169 and Arg171. The carbonyl oxygen of Gly69 forms a hydrogen bond with the main chain amide nitrogen of Gly72, thus stabilizing the conformation of the "bulge 1" in the loop L1. The side chains of Arg68 and Tyr104 are in close proximity and form a cation-π interaction. Arg103 and Asp108 are involved in a relay of hydrogen bonds among Try58, Ala71 and Arg171 (Fig. 3). The combination of all these interactions likely maintains the construction of the "loop-tip surface".

Noteworthy, in sharp contrast with Asp78 and Arg171 that respectively have a solvent accessible surface area (SASA) of 92.3 and 128.2 $Å^2$, the surface center residues Asp108 and Arg103 are nearly buried with an SASA of 14.3 and 37.4 $Å^2$, respectively. This implicates that mutation of either Asp108 or Arg103 would likely alter the structure of the "loop-tip surface". Meanwhile, due to residence of the salt-bridged residues Asp108 and Arg103, the surface center is approximately neutralized (Fig. S3). In comparison, the edge of the "loop-tip surface" has considerable electrostatic potential, since its two adjacent sides of the barrel-like domain are distributed with positively or negatively charged patches (Fig. S3).

Also, it is worthy to mention that the residues on the "loop-tip surface" of human CASPR2 Disc domain, except S55, R68 and G69, have relatively low conservation among the five CASPR subfamily members CASPR1-CAPSR5 (Fig. 3B and Fig. S4). Indeed, the residues on the side surface of human CASPR2 Disc domain, such as Arg114 and Arg160 that constitute a positively charged region (Fig. S3B), also have low conservation. This suggests that the Disc domains of the CASPR subfamily have diverse surface properties although the subfamily members might have a conserved topology. The diversity in surface property of the Disc domain in the CASPR subfamily members might confer specificity in their autoantibody recognition.

3.4. Structure-based epitope prediction and mutagenesis

In order to dissect key residues in the epitope(s) within human CASPR2 Disc domain, we first applied its crystal structure to DiscoTope 2.0 server [44] for epitope prediction. Six regions with high DiscoTope scores above the default value of −3.7 are, from the N-terminus of the Disc domain, sequentially named Epitope-1 through Epitope-6 (Fig. 4A). The predicted Epitope-1 (covering residues 52-57), Epitope-2 (residues 68-72) and Epitope-3 (residues 76-84) fall into the loop L1 of the Disc domain, while the Epitope-4 mainly includes residues 103-112 that corresponds to the loop L2. The residues from the protruding hairpin (βC and βD), the barrel wall strand β5, and the loop L3 (residues 140-144) are predicted to constitute the Epitope-5. The Epitope-

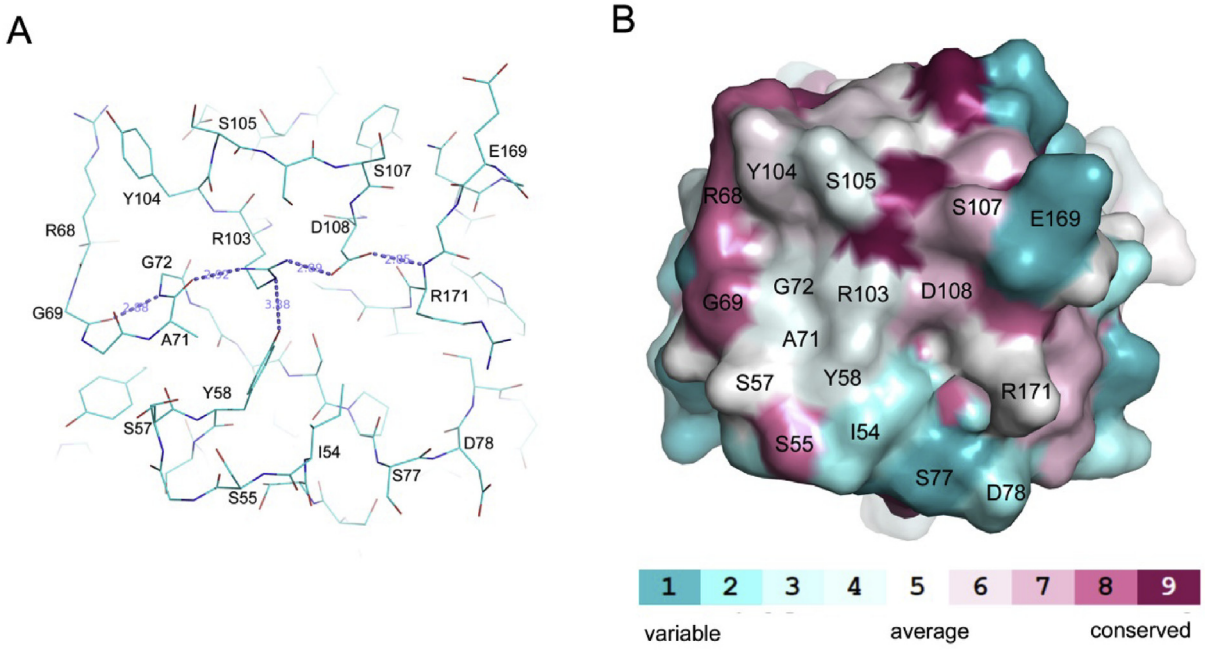

Fig. 3. Residues distributed over the "loop-tip surface" of human CASPR2 Disc domain. (A) Line representation of the residues with hydrogen bonds shown in slate dotted lines. (B) Conservation of each residue among the CASPR subfamily members, CASPR1-5, mapped to the CASPR2 Disc domain surface. Bottom is shown a scale for conservation degree.

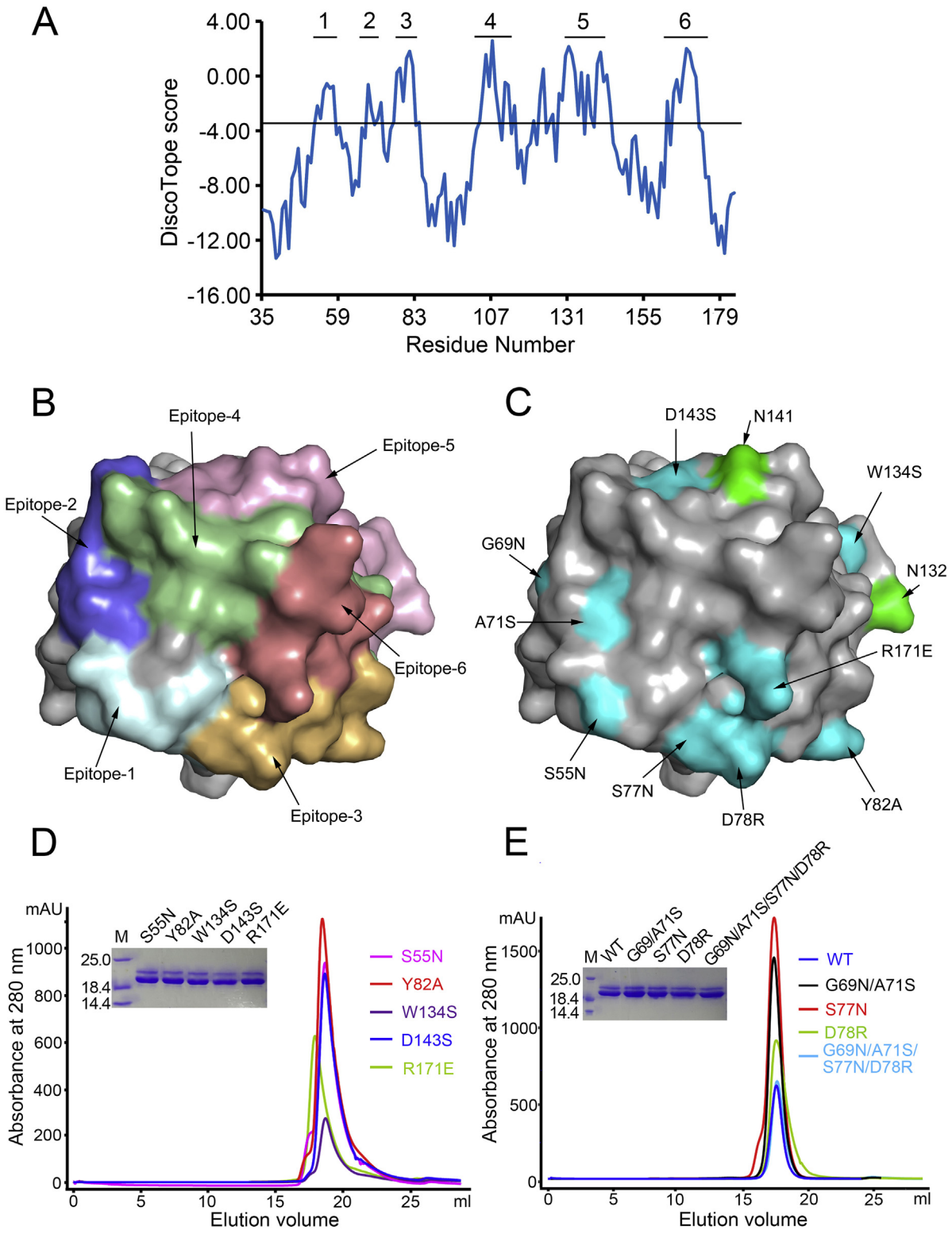

Fig. 4. Structure-based epitope prediction and mutagenesis of human CASPR2 Disc domain. (A) A plot of DiscoTope score (represented by the vertical axis) versus residue number (by the horizontal axis). (B) Predicted epitopes mapped on the Disc domain surface (in grey). Color code: Epitope-1, pale cyan; Epitope-2, slate; Epitope-3, light orange; Epitope-4, pale green; Epitope-5, light pink; Epitope-6, salmon. (C) Mutations mapped on the Disc domain surface and colored in cyan, with S55N located in Epitope-1, G69N/A71S in Epitope-2, S77N, D78R and Y82A in Epitope-3, W134S and D143S in Epitope-5, and R171E in Epitope-6. Two potential N-linked glycosylation sites N132 and N141 are colored in green. The Disc domain in the panels B and C has the same orientation that is related to Fig. 1B by 90° along the vertical axis. (D–E) Gel filtration chromatograms of the wild-type (WT) human CASPR2 Disc domain and its mutants, with S55N, Y82A, W134S, D143S and R171E displayed in the panel D, and G69N/A71S, S77N, D78R, and G69N/A71S/S77N/D78R shown in the panel E. The insets are indicated for SDS-PAGE analysis of the recombinant proteins. The lane M is for molecular weight markers in kDa. (For interpretation of the references to color in this figure legend, the reader is referred to the Web version of this article.)

6 is supposed to cover residues 164-171 that reside in the loop L4. In short, the loop region defined by L1-L4 on one end of the barrel-like Disc domain constitutes the majority of the predicted epitopes.

Correspondingly, we prepared nine mutants of human CASPR2 Disc domain plus the N-terminal segment (residues 28-181). The mutations S55N, G69N/A71S, S77N, D78R and Y82A, were located in the loop L1 and distributed in three predicted epitopes, Epitopes 1-3 (Fig. 4). The mutations W134S and D143S occurred in the Epitope-5, while R171E was located in the Epitope-6. Supposedly, the mutations S55N, G69N/A71S, S77N, W134S and D143S would each introduce N-linked glycans that may act as a wedge to block interaction between human CASPR2 and auto-antibodies. For the mutations W134S and D143S, the N-linked glycans would be attached to N132 and N141, respectively (Fig. 4C). In addition, we created a quadruple mutant that combined the G69N, A71S, S77N and D78R mutations. All of the nine mutants, like the wild-type protein, were expressed well in baculovirus-transduced mammalian cells, and purified into high purity as demonstrated by SDS-PAGE analysis (Fig. 4D and E). Also, all of them exhibited a similar chromatographic peak on a gel-filtration column, indicating that they have similar physical property, such as monodispersity, in solution (Fig. 4D and E). For an unknown reason, these mutants and their wild-type counterpart (including residues 28-181) migrated as two bands on an SDS-PAGE gel, whereas the construct (including residues 35-181) used for crystallization ran as a single band.

3.5. Protein-based ELISA revealed hot spots for autoantibody recognition

Using three rounds of protein-based ELISA assays, we tested if the above mentioned mutations are able to alter interactions between CASPR2 Disc domain and CASPR2 autoantibodies from LE patients. In the ELISA assays, an OD_{450} value is supposed to be proportional to CASPR2 autoantibodies bound to the coated Disc protein. In the first round ELISA assay, CSF from the patient 1 (Pat1, recognizing only Disc-Lam1 domains on CASPR2) was tested at a series of dilutions against eight mutants S55N, G69N/A71S, S77N, D78R, Y82A, W134S, D143S and R171E. Upon either G69N/A71S, S77N or D78R mutations, the binding of Pat1 autoantibodies at a 1:40 dilution to human CASPR2 Disc domain was decreased by ~22% for G69N/A71S, ~28% for S77N and ~31% for D78R in comparison with the wild-type protein (Fig. 5). For the D78R mutant, Pat1 autoantibodies binding to the D78R mutant was decreased by 20–30%, while OD difference was only found at dilutions of 1:40 and 1:80. In contrast, other mutations hardly altered the binding of Pat1 autoantibodies to CASPR2 Disc domain at any dilutions (Fig. 5).

In the second round of ELISA assay, we focused on the mutants of G69N/A71S, S77N and D78R for twelve LE patients including Pat1. Meanwhile, a quadruple mutant of G69N/A71S/S77N/D78R was also included. As indicated in Table 2, CSF antibody titers were variable among patients ranging from 1:320 to 1:10240. All patients' CSF was diluted based on their autoantibody titer at a ratio between 1:10 and 1:100 for ELISA assay (Fig. 6A). For patients Pat2, Pat3, Pat4, Pat8 and Pat9 with CSF diluted at different folds, the four mutations in Disc domain decreased OD_{450} to considerable extents as observed for Pat1 (Fig. 6A). In order to compare the percentage of OD decrease between mutant and wild-type Disc domain protein among these patients with different CSF titers, we chose for each patient the dilution that gave an OD around 0.8 for the wild-type protein. In comparison with the wild-type CASPR2 protein, the quadruple mutant was found to present an OD_{450} decrease of 15%–70% in binding to autoantibodies from eleven patients out of twelve LE patients tested (Fig. 6B and C). Especially, for Pat1 and Pat3, a decrease of 72% and 70% was observed in OD_{450} for the quadruple mutant, implicating that the four residues G69, A71, S77 and D78 have a synergic impact on autoantibody recognition (Fig. 6B and C). The quadruple mutant also significantly impaired autoantibodies binding (from 38% to 51% decrease) to CASPR2 Disc domain for Pat2, Pat4, Pat8 and Pat9. In addition, for the Pat1, Pat2 and Pat3, both S77N and D78R mutations significantly decreased autoantibodies binding to CASPR2 (Fig. 6B and C). Notably, Pat1, Pat2, Pat3 and Pat4 autoantibodies have been previously shown to target Disc-Lam1 domains of CASPR2 only, while Pat8 and Pat9 autoantibodies target multiple domains of CASPR2 (Table 2) [18]. The quadruple mutation consistently impaired Disc domain binding to autoantibodies from these patients (Fig. 6B and C), suggesting that anti-CASPR2 autoantibodies might share the same epitope in Disc domain.

In the third round of ELISA assay, we compared “relative affinity” of CSF autoantibodies in binding to the wild-type and quadruple mutant Disc domain. Taking into account of that a large amount of CSF sample will be needed to obtain a binding curve with a saturation phase for determining a relative affinity, we selected high-titer Pat5 CSF. Given that the same amount of CSF autoantibodies was added in plates, the maximal OD_{450} should be identical for the wild-type and mutant Disc domain to reach in a saturated phase. In order to characterize the relative affinity, “q50” was used to correspond to the quantity of protein where 50% of maximal OD_{450} is reached. As shown in Fig. 7, a q50 value of 0.07 μg was estimated for the wild-type protein. In contrast, for the quadruple mutant we obtained a q50 value of 0.14 μg. These results indicated that Pat5 CSF presented lower binding affinity with the quadruple mutant than the wild-type Disc domain, and further verified that the spots at the G69, A71, S77 and D78 in Disc domain are determinant for LE autoantibody recognition.

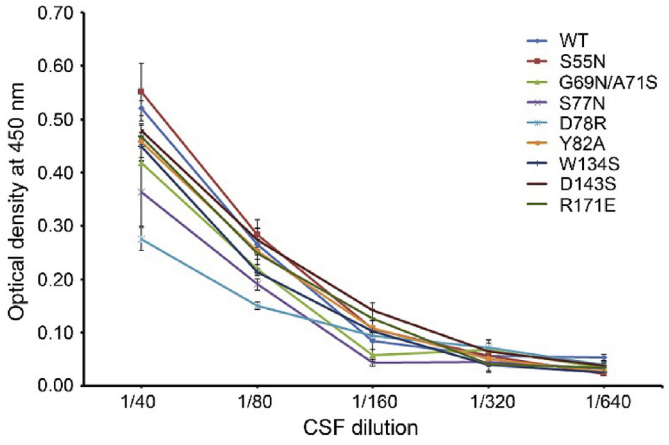

Fig. 5. Protein-based ELISA analysis for Pat1 CSF autoantibodies at the indicated dilutions binding to human CASPR2 Disc domain wild-type and eight mutants.

4. Discussion

Autoantibodies directed against CASPR2 have been associated with a long list of neurological immune disorders including limbic encephalitis. Recently we have found that anti-CASPR2 antibodies in the CSF are prone to occur in a subtype of autoimmune encephalitis with limbic involvement and seizures [18]. Although CASPR2 contains different epitopes within the extracellular region [54], we and other have shown that autoantibodies appear to predominantly target the N-terminal region of CASPR2 and that the Disc domain harbors a major epitope [32,33]. Coincidentally, it is the Disc domain that structurally distinguishes the CASPR subfamily from the others in the neurexin superfamily. Structural mapping of autoepitopes within human CASPR2 Disc domain will reveal how autoantibodies affect multifaceted functions and extensive protein interactions of CASPR2.

Using the emerging technology of baculovirus-transduced mammalian cells that we have successfully used for structural biology of glycoproteins [37,55], we fulfilled high expression of human CASPR2 Disc domain as well as its derivates. The crystal structure of human CASPR2 Disc domain was determined to a high resolution of 1.31 Å,

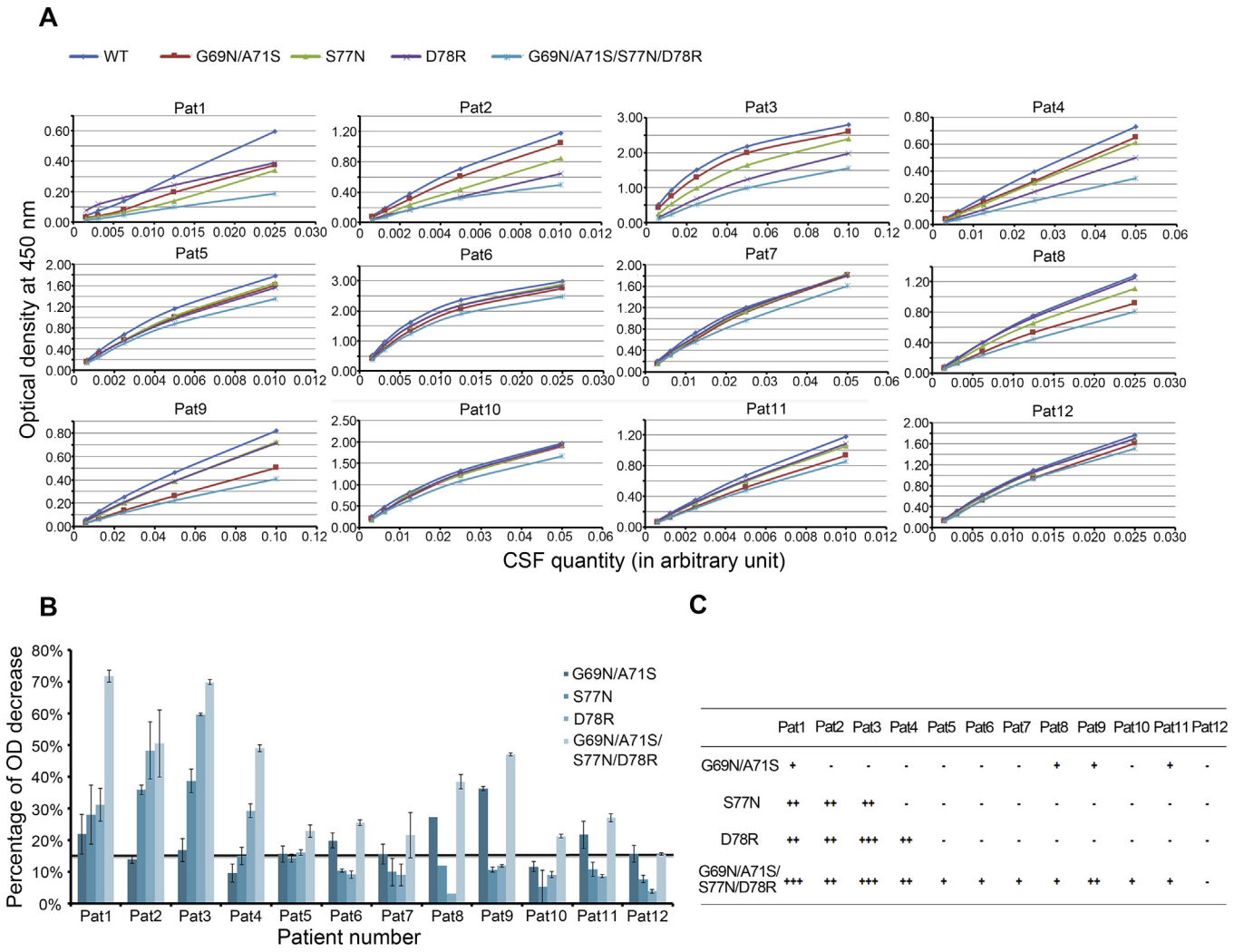

Fig. 6. Protein-based ELISA analysis for 12 LE patients CSF binding to Disc domain and its four variants. (A) Binding of CSF autoantibodies from patients (Pat1 ~ Pat12) at the indicated arbitrary unit of antibody quantity to Disc domain wild-type and mutants. Herein, an arbitrary unit refers to the reciprocal of dilution fold. (B) Percentage of optical density (OD) decrease for the binding of anti-CASPR2 antibodies from twelve LE patients on the indicated mutant versus the wide-type CASPR2 Disc domain. For the patient 9, anti-CASPR2 binding to the mutants G69N/A71S, S77N and D78R was only tested once. (C) Summary of mutations and their impairment on CASPR2 Disc binding to CSF from patients. "+ + +", strong; "+ +", medium; "+", weak; "-", ignorable.

partially due to high purity and monodispersity of the recombinant protein. To our best knowledge, this is the first atomic-resolution structure of the CASPR subfamily members, which reveals that the Disc domain assumes a totally all β structure with a conserved disulfide-bond interlocking its N- and C-termini.

Although human CASPR2 Disc domain and coagulation factor V C2 domain share a barrel-like topology, their loops connecting the barrel-wall β-strands have variable conformations. In human coagulation

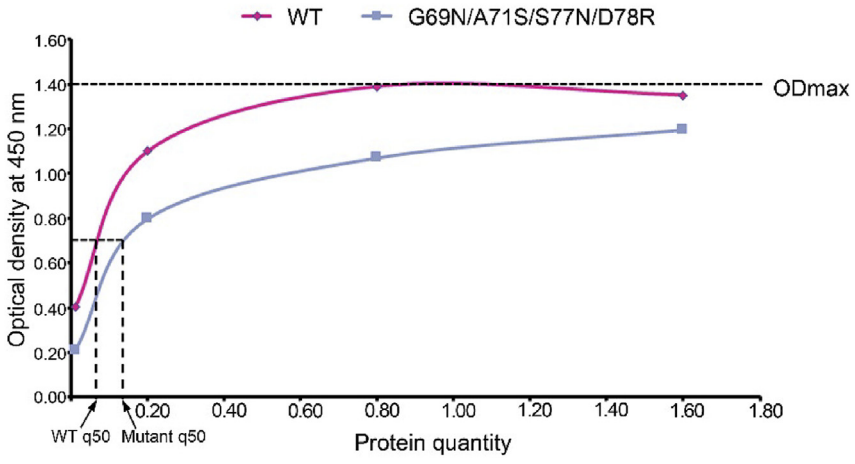

Fig. 7. Binding curves of Pat5 CSF against coated Disc domain wild-type and quadruple mutant G69N/A71S/S77N/D78R. The horizontal coordinate axis represents the protein quantity used to coat the 96-well plates. 0.01, 0.2, 0.8 and 1.6 μg of Disc domain wild-type or quadruple mutant were respectively used to coat the plates, while the same amount of Pat CSF (diluted at 1:100) was added to each well. The relative affinity is represented by "q50" which corresponds to the quantity of protein where 50% of maximal OD_{450} is reached. Given that the same amount of CSF autoantibodies was added, the maximal OD_{450} for the wild-type and mutant Disc domain should be identical and thus labeled as "ODmax". Due to limitation in CSF source, this experiment was performed only once.

factor V C2 domain, loops protrude like spikes out of one end of the barrel and form a predominantly positive-charge region for membrane-binding [40]. In contrast, human CASPR2 Disc domain defines the counterpart end using four loops L1-L4 to constitute a relatively flat surface, named “loop-tip surface”, which is basically neutral in the center and has considerable electrostatic potential on the edge. Such a surface property likely confers human CASPR2 Disc domain binding to other proteins including autoantibodies, similar to the case of DDR2 Disc domain [52]. Consistently, the predicted epitopes by DiscoTope within human CASPR2 Disc domain also point to the “loop-tip surface” and adjacent barrel-wall surfaces (Fig. 4).

Since LE patient CSF samples were truly limited, we adopted three rounds of EILSA assays to investigate which hot spots in CASRP2 Disc domain are critical for CSF autoantibody recognition. In the first round, we used one patient's CSF to screen Disc mutants. Among the eight mutants S55N, G69N/A71S, S77N, D78R, Y82A, W134S, D143S and R171E, three mutants G69N/A71S, S77N and D78R impaired Pat1's CSF autoantibodies binding to the CASPR2 Disc domain (Fig. 5). In the second round, we focused on the three mutants plus their combination. The quadruple mutant of G69N/A71S/S77N/D78R showed a decreased binding for 11 out of 12 LE patients' CSF autoantibodies (Fig. 6). Meanwhile, anti-CASPR2 autoantibodies from two types of LE patients might share the same epitope in Disc domain, since the quadruple mutant impaired Disc binding to autoantibodies not only from patients Pat1, Pat2, Pat3 and Pat4, but also from Pat8 and Pat9 (Fig. 6). Furthermore, the quadruple mutations occur to the “loop-tip-surface” of Disc domain, which implicates that LE patient CSF autoantibodies might bind to Disc domain in a single-epitope fashion. From this point of view, it is reasonable to quantitatively measure a relative affinity of Disc domain binding to CSF although it is a complex mixture of anti-CASPR2 autoantibodies. Therefore, in the third round of ELISA assay, we tried to compare “relative affinity” of CSF autoantibodies in binding to the wild-type and quadruple mutant Disc domain (Fig. 7). Due to limited CSF sample availability, we selected CSF from the patient Pat5 that had highest titer of autoantibodies, coated different amounts of Disc protein in plates, and put forward to the phrase “q50” to present the relative affinity (Fig. 7). The higher q50 value for the quadruple mutant Disc domain means its lower affinity for Pat5 CSF autoantibodies. This result further verified that the spots at the G69, A71, S77 and D78 in Disc domain are determinant for LE autoantibody recognition. Stated differently, the ELISA assay results indicate that the “loop-tip surface” in human CASPR2 Disc domain bears hot spots for LE autoantibodies recognition. Different from either G69N/A71S or S77N mutations that likely introduced N-linked glycans as steric hindrance for antigen-antibody interaction, the charge-reversal mutation of D78R implicated that CASPR2 recognition by autoantibodies in LE patients likely depends on electrostatic complementarity. Interestingly, these hot spots are located on the loop L1. Intrinsic flexibility of this loop might increase the capacity for movement to form strong antigen-antibody interactions by “induced fit” [56]. Indeed, flexibility appears to be a structural feature associated with epitope sites on autoantigenic molecules [57,58].

Recently, some authors showed that anti-CASPR2 antibodies associated with limbic encephalitis mainly target hippocampal inhibitory interneurons and may induce alteration of CASPR2-mediated inhibitory synaptic contacts [32]. It was reported that *in utero* exposure to CASPR2-directed autoantibodies cloned from a mother of an ASD child can lead to an ASD-like phenotype in mice [11], although this observation seemed controversial [59]. Adult CASPR2 KO mice exhibited a significant decrease in the number of inhibitory interneurons and ASD-like behavioral abnormalities [28]. Thus, it seems that anti-CASPR2 autoantibodies could play a fundamental role in the pathogenic processes through a functional effect on CASPR2 [18], which is similar to the effects exerted through gene knockout. Since functions of CASPR2 may operate via interactions with other proteins such as TAG-1 and the VGKC complex subunits [1,21,60,61], we propose that CASPR2 autoantibodies would compete with these proteins for CASPR2 binding. Indeed, it was shown that CASPR2 autoantibodies were able to decrease CASPR2-TAG-1 association in ELISA [62].

As revealed by electron microscopy, the N-terminal domains, including the Disc domain, of CASPR2 form a large lobe that deviates from the main body of molecular architecture [34]. Such a domain arrangement would facilitate exposure of the “loop-tip surface” of the Disc domain for interactions with an endogenous ligand or autoantibodies. From this point, future searching for the endogenous ligand of CASPR2 might be based on the Disc domain. A caveat for this strategy is that autoantibodies against CASPR2 target other regions beyond the Disc domain [18]. The fact that CASPR2 has multiple autoepitopes may explain that Pat12 autoantibodies maintained its binding to the quadruple mutant in the protein-based ELISA assay. This may also underlie the fact that autoantibodies against CASPR2 associate with a wide spectrum of symptoms, including limbic or more extensive encephalitis [63]. Given that autoantibodies from a subset of LE patients may target the Disc domain of CASPR2 and would likely compete with a potential endogenous ligand, some autoantibodies in a wider range of pathogenic conditions might direct against multiple domains of CASPR2 and antagonize interactions with other proteins.

In summary, we have determined the crystal structure of human CASPR2 Disc domain and found that the quadruple mutant G69N/A71S/S77N/D78R impaired CASPR2 binding to autoantibodies from 11 out of 12 LE patients. These findings indicate that the loop L1 in the Disc domain bears hot spots for LE autoantibody interaction. Together with our previous study [32], structural mapping of autoepitopes within human CASPR2 Disc domain sheds light on how autoantibodies might affect CASPR2 functions in the pathological contexts such as limbic encephalitis.

Conflicts of interest

The authors declare that they have no conflicts of interest with the contents of this article.

Author contributions

HL and JH conceived the project, coordinated the study, analyzed the data and wrote the manuscript. WL, JZ, MS, FX, NN and JL performed the experiments, analyzed the data and contributed to manuscript preparation.

Acknowledgements

This work was supported by grants to Heli Liu from “Thousand Talents Program” and National Natural Science Foundation of China (grants No. 81322047 and 81673525), and by grants to Jérôme Honnorat from Agence Nationale de la Recherche (ANR-14-CE15-0001-MECANO), and FRM (Fondation pour la Recherche Médicale) DQ20170336751. Atomic coordinates and structure factor for human CASPR2 Disc domain have been deposited in the Protein Data Bank (PDB) under accession number 5Y4M.

Appendix A. Supplementary data

Supplementary data to this article can be found online at https://doi.org/10.1016/j.jaut.2018.09.012.

References

[1] A. Van Sonderen, M. Petit-Pedrol, J. Dalmau, M.J. Titulaer, The value of LGI1, Caspr2 and voltage-gated potassium channel antibodies in encephalitis, Nat. Rev. Neurol. 13 (2017) 290–301.
[2] A. Chefdeville, J. Honnorat, C.S. Hampe, V. Desestret, Neuronal central nervous system syndromes probably mediated by autoantibodies, Eur. J. Neurosci. 43 (2016) 1535–1552.

[3] J.J. Linnoila, M.R. Rosenfeld, J. Dalmau, Neuronal surface antibody-mediated autoimmune encephalitis, Semin. Neurol. 34 (2014) 458–466.
[4] S.R. Irani, S. Alexander, P. Waters, K.A. Kleopa, P. Pettingill, L. Zuliani, et al., Antibodies to Kv1 potassium channel-complex proteins leucine-rich, glioma inactivated 1 protein and contactin-associated protein-2 in limbic encephalitis, Morvan's syndrome and acquired neuromyotonia, Brain 133 (2010) 2734–2748.
[5] M. Lai, M.G. Huijbers, E. Lancaster, F. Graus, L. Bataller, R. Balicegordon, et al., Investigation of LGI1 as the antigen in limbic encephalitis previously attributed to potassium channels: a case series, Lancet Neurol. 9 (2010) 776–785.
[6] A. Vincent, S.R. Irani, Caspr2 antibodies in patients with thymomas, J. Thorac. Oncol. 5 (2010) S277–S280.
[7] E.B. Becker, L. Zuliani, R. Pettingill, B. Lang, P. Waters, A. Dulneva, et al., Contactin-associated protein-2 antibodies in non-paraneoplastic cerebellar ataxia, J. Neurol. Neurosurg. Psychiatry 83 (2012) 437–440.
[8] B. Joubert, F. Gobert, L. Thomas, M. Saint-Martin, V. Desestret, P. Convers, et al., Autoimmune episodic ataxia in patients with anti-CASPR2 antibody-associated encephalitis, Neurol. Neuroimmunol. Neuroinflamm. 4 (2017) e371.
[9] C.J. Klein, V.A. Lennon, P.A. Aston, A. Mckeon, S.J. Pittock, Chronic pain as a manifestation of potassium channel-complex autoimmunity, Neurology 79 (2012) 1136.
[10] R.E. Rosch, A. Bamford, Y. Hacohen, E. Wraige, A. Vincent, L. Mewasingh, et al., Guillain-Barre syndrome associated with CASPR2 antibodies: two paediatric cases, J. Peripher. Nerv. Syst. 19 (2014) 246–249.
[11] L. Brimberg, S. Mader, V. Jeganathan, R. Berlin, T.R. Coleman, P.K. Gregersen, et al., Caspr2-reactive antibody cloned from a mother of an ASD child mediates an ASD-like phenotype in mice, Mol. Psychiatr. 21 (2016) 1663–1671.
[12] F. Govert, K. Witt, R. Erro, H. Hellriegel, S. Paschen, E. Martinez-Hernandez, et al., Orthostatic myoclonus associated with Caspr2 antibodies, Neurology 86 (2016) 1353–1355.
[13] J. Suleiman, S. Wright, D. Gill, F. Brilot, P. Waters, K. Peacock, et al., Autoantibodies to neuronal antigens in children with new-onset seizures classified according to the revised ILAE organization of seizures and epilepsies, Epilepsia 54 (2013) 2091–2100.
[14] S. Wright, A.T. Geerts, C.M. Jol-van der Zijde, L. Jacobson, B. Lang, P. Waters, et al., Neuronal antibodies in pediatric epilepsy: clinical features and long-term outcomes of a historical cohort not treated with immunotherapy, Epilepsia 57 (2016) 823–831.
[15] G. Unverengil, E.N. Vanli Yavuz, E. Tuzun, E. Erdag, S. Kabadayi, B. Bilgic, et al., Brain infiltration of immune cells in CASPR2-antibody associated mesial temporal lobe epilepsy with hippocampal sclerosis, Noro Psikiyatr Ars 53 (2016) 344–347.
[16] J. Song, S. Jing, C. Quan, J. Lu, X. Qiao, K. Qiao, et al., Isaacs syndrome with CASPR2 antibody: a series of three cases, J. Clin. Neurosci. 41 (2017) 63–66.
[17] Z. Karaaslan, E. Ekizoglu, P. Tekturk, E. Erdag, E. Tuzun, N. Bebek, et al., Investigation of neuronal auto-antibodies in systemic lupus erythematosus patients with epilepsy, Epilepsy Res. 129 (2017) 132–137.
[18] B. Joubert, M. Saint-Martin, N. Noraz, G. Picard, V. Rogemond, F. Ducray, et al., Characterization of a subtype of autoimmune encephalitis with anti-contactin-associated protein-like 2 antibodies in the cerebrospinal fluid, prominent limbic symptoms, and seizures, JAMA Neurol. 73 (2016) 1115–1124.
[19] S. Poliak, L. Gollan, R. Martinez, A. Custer, S. Einheber, J.L. Salzer, et al., Caspr2, a new member of the neurexin superfamily, is localized at the juxtaparanodes of myelinated axons and associates with K+ channels, Neuron 24 (1999) 1037–1047.
[20] T.C. Sudhof, Synaptic neurexin complexes: a molecular code for the logic of neural circuits, Cell 171 (2017) 745–769.
[21] G.R. Anderson, T. Galfin, W. Xu, J. Aoto, R.C. Malenka, T.C. Sudhof, Candidate autism gene screen identifies critical role for cell-adhesion molecule CASPR2 in dendritic arborization and spine development, Proc. Natl. Acad. Sci. U. S. A. 109 (2012) 18120–18125.
[22] O. Varea, M.D. Martin-de-Saavedra, K.J. Kopeikina, B. Schurmann, H.J. Fleming, J.M. Fawcett-Patel, et al., Synaptic abnormalities and cytoplasmic glutamate receptor aggregates in contactin associated protein-like 2/Caspr2 knockout neurons, Proc. Natl. Acad. Sci. U. S. A. 112 (2015) 6176–6181.
[23] A. Gdalyahu, M. Lazaro, O. Penagarikano, P. Golshani, J.T. Trachtenberg, D.H. Geschwind, The Autism Related Protein Contactin-Associated Protein-Like 2 (CNTNAP2) Stabilizes New Spines: an In Vivo Mouse Study, PloS One 10 (2015) e0125633.
[24] K.A. Strauss, E.G. Puffenberger, M.J. Huentelman, S. Gottlieb, S.E. Dobrin, J.M. Parod, et al., Recessive symptomatic focal epilepsy and mutant contactin-associated protein-like 2, N. Engl. J. Med. 354 (2006) 1370–1377.
[25] B. Bakkaloglu, B.J. O'Roak, A. Louvi, A.R. Gupta, J.F. Abelson, T.M. Morgan, et al., Molecular cytogenetic analysis and resequencing of contactin associated protein-like 2 in autism spectrum disorders, Am. J. Hum. Genet. 82 (2008) 165–173.
[26] A.J. Verkerk, C.A. Mathews, M. Joosse, B.H. Eussen, P. Heutink, B.A. Oostra, CNTNAP2 is disrupted in a family with Gilles de la Tourette syndrome and obsessive compulsive disorder, Genomics 82 (2003) 1–9.
[27] M. Saint-Martin, B. Joubert, V. Pellier-Monnin, O. Pascual, N. Noraz, J. Honnorat, Contactin-associated protein-like 2, a protein of the neurexin family involved in several human diseases, Eur. J. Neurosci. 48 (2018) 1906–1923.
[28] O. Penagarikano, B.S. Abrahams, E.I. Herman, K.D. Winden, A. Gdalyahu, H. Dong, et al., Absence of CNTNAP2 leads to epilepsy, neuronal migration abnormalities, and core autism-related deficits, Cell 147 (2011) 235–246.
[29] E. Peles, M. Nativ, M. Lustig, M. Grumet, J. Schilling, R. Martinez, et al., Identification of a novel contactin-associated transmembrane receptor with multiple domains implicated in protein-protein interactions, EMBO J. 16 (1997) 978–988.
[30] M. Poot, Connecting the CNTNAP2 networks with neurodevelopmental disorders, Mol. Syndromol. 6 (2015) 7–22.
[31] N. Sinmaz, T. Nguyen, F. Tea, R.C. Dale, F. Brilot, Mapping autoantigen epitopes: molecular insights into autoantibody-associated disorders of the nervous system, J. Neuroinflammation 13 (2016) 219.
[32] D. Pinatel, B. Hivert, J. Boucraut, M. Saint-Martin, V. Rogemond, L. Zoupi, et al., Inhibitory axons are targeted in hippocampal cell culture by anti-Caspr2 autoantibodies associated with limbic encephalitis, Front. Cell. Neurosci. 9 (2015) 265.
[33] A.L. Olsen, Y. Lai, J. Dalmau, S.S. Scherer, E. Lancaster, Caspr2 autoantibodies target multiple epitopes, Neurol. Neuroimmunol. Neuroinflamm. 2 (2015) e127.
[34] Z. Lu, M.V. Reddy, J. Liu, A. Kalichava, J. Liu, L. Zhang, et al., Molecular architecture of contactin-associated protein-like 2 (CNTNAP2) and its interaction with contactin 2 (CNTN2), J. Biol. Chem. 291 (2016) 24133–24147.
[35] E.N. Rubio-Marrero, G. Vincelli, C.M. Jeffries, T.R. Shaikh, I.S. Pakos, F.M. Ranaivoson, et al., Structural characterization of the extracellular domain of CASPR2 and insights into its association with the novel ligand Contactin1, J. Biol. Chem. 291 (2016) 5788–5802.
[36] A. Dukkipati, H.H. Park, D. Waghray, S. Fischer, K.C. Garcia, BacMam system for high-level expression of recombinant soluble and membrane glycoproteins for structural studies, Protein Expr. Purif. 62 (2008) 160–170.
[37] H. Liu, Z.S. Juo, A.H. Shim, P.J. Focia, X. Chen, K.C. Garcia, et al., Structural basis of semaphorin-plexin recognition and viral mimicry from Sema7A and A39R complexes with PlexinC1, Cell 142 (2010) 749–761.
[38] Z. Otwinowski, W. Minor, Processing of X-ray diffraction data collected in oscillation mode, Methods Enzymol. 276 (1997) 307–326.
[39] A.J. McCoy, Solving structures of protein complexes by molecular replacement with phaser, Acta Crystallogr. D Biol. Crystallogr. 63 (2007) 32–41.
[40] S. Macedo-Ribeiro, W. Bode, R. Huber, M.A. Quinn-Allen, S.W. Kim, T.L. Ortel, et al., Crystal structures of the membrane-binding C2 domain of human coagulation factor V, Nature 402 (1999) 434–439.
[41] P.D. Adams, P.V. Afonine, G. Bunkoczi, V.B. Chen, I.W. Davis, N. Echols, et al., PHENIX: a comprehensive Python-based system for macromolecular structure solution, Acta Crystallogr. D Biol. Crystallogr. 66 (2010) 213–221.
[42] P. Emsley, K. Cowtan, Coot: model-building tools for molecular graphics, Acta Crystallogr. D Biol. Crystallogr. 60 (2004) 2126–2132.
[43] V.B. Chen, W.B. Arendall 3rd, J.J. Headd, D.A. Keedy, R.M. Immormino, G.J. Kapral, et al., MolProbity: all-atom structure validation for macromolecular crystallography, Acta Crystallogr. D Biol. Crystallogr. 66 (2010) 12–21.
[44] J.V. Kringelum, C. Lundegaard, O. Lund, M. Nielsen, Reliable B cell epitope predictions: impacts of method development and improved benchmarking, PLoS Comput. Biol. 8 (2012) e1002829.
[45] L. Holm, P. Rosenstrom, Dali server: conservation mapping in 3D, Nucleic Acids Res. 38 (2010) W545–W549.
[46] M.A. Larkin, G. Blackshields, N.P. Brown, R. Chenna, P.A. McGettigan, H. McWilliam, et al., Clustal W and clustal X version 2.0, Bioinformatics 23 (2007) 2947–2948.
[47] P. Gouet, E. Courcelle, D.I. Stuart, F. Metoz, ESPript: analysis of multiple sequence alignments in PostScript, Bioinformatics 15 (1999) 305–308.
[48] H. Ashkenazy, S. Abadi, E. Martz, O. Chay, I. Mayrose, T. Pupko, et al., ConSurf 2016: an improved methodology to estimate and visualize evolutionary conservation in macromolecules, Nucleic Acids Res. 44 (2016) W344–W350.
[49] M.D. Winn, C.C. Ballard, K.D. Cowtan, E.J. Dodson, P. Emsley, P.R. Evans, et al., Overview of the CCP4 suite and current developments, Acta Crystallogr. D Biol. Crystallogr. 67 (2011) 235–242.
[50] G. Falivelli, A. De Jaco, F.L. Favaloro, H. Kim, J. Wilson, N. Dubi, et al., Inherited genetic variants in autism-related CNTNAP2 show perturbed trafficking and ATF6 activation, Hum. Mol. Genet. 21 (2012) 4761–4773.
[51] B.W. Matthews, Solvent content of protein crystals, J. Mol. Biol. 33 (1968) 491.
[52] F. Carafoli, D. Bihan, S. Stathopoulos, A.D. Konitsiotis, M. Kvansakul, R.W. Farndale, et al., Crystallographic insight into collagen recognition by discoidin domain receptor 2, Structure 17 (2009) 1573–1581.
[53] P.C. Spiegel Jr., M. Jacquemin, J.M. Saint-Remy, B.L. Stoddard, K.P. Pratt, Structure of a factor VIII C2 domain-immunoglobulin G4kappa Fab complex: identification of an inhibitory antibody epitope on the surface of factor VIII, Blood 98 (2001) 13–19.
[54] D.F. Obregon, Y.Y. Zhu, A.R. Bailey, S.M. Portis, H.Y. Hou, J. Zeng, et al., Potential autoepitope within the extracellular region of contactin-associated protein-like 2 in mice, Br. J. Med. Med. Res. 4 (2014) 416.
[55] Z. Lin, J. Liu, H. Ding, F. Xu, H. Liu, Structural basis of SALM5-induced PTPÎ' dimerization for synaptic differentiation, Nat. Commun. 9 (2018) 268.
[56] J.M. Rini, U. Schulze-Gahmen, I.A. Wilson, Structural evidence for induced fit as a mechanism for antibody-antigen recognition, Science 255 (1992) 959–965.
[57] P.H. Plotz, The autoantibody repertoire: searching for order, Nat. Rev. Immunol. 3 (2003) 73–78.
[58] Y. Arafat, G. Fenalti, J.C. Whisstock, I.R. Mackay, M. Garcia de la Banda, M.J. Rowley, et al., Structural determinants of GAD antigenicity, Mol. Immunol. 47 (2009) 493–505.
[59] E.J.L. Coutinho, M.G. Pedersen, M.E. Benros, B. Nørgaard-Pedersen, P.B. Mortensen, P.J. Harrison, A. Vincent, CASPR2 autoantibodies are raised during pregnancy in mothers of children with mental retardation and disorders of psychological development but not autism, J. Neurol. Neurosurg. Psychiatry 88 (2017) 4.
[60] N. Chen, F. Koopmans, A. Gordon, I. Paliukhovich, R.V. Klaassen, R.C. van der Schors, et al., Interaction proteomics of canonical Caspr2 (CNTNAP2) reveals the presence of two Caspr2 isoforms with overlapping interactomes, Biochim. Biophys. Acta 1854 (2015) 827–833.
[61] M. Traka, L. Goutebroze, N. Denisenko, M. Bessa, A. Nifli, S. Havaki, et al., Association of TAG-1 with Caspr2 is essential for the molecular organization of juxtaparanodal regions of myelinated fibers, J. Cell Biol. 162 (2003) 1161–1172.
[62] K.R. Patterson, J. Dalmau, E. Lancaster, Mechanisms of Caspr2 antibodies in autoimmune encephalitis and neuromyotonia, Ann. Neurol. 83 (2018) 40–51.
[63] M.T. Montojo, M. Petit-Pedrol, F. Graus, J. Dalmau, Clinical spectrum and diagnostic value of antibodies against the potassium channel related protein complex, Neurologia 30 (2015) 295–301.